A triple GEM detector
with two dimensional readout

M. Ziegler, P. Sievers, U. Straumann

Physik Institut Universität Zürich

February 7, 2008

This is a reduced version for hep-ex, from which the large photographs have been
omitted to keep it small in size. A full version is available from:
http://www.physik.unizh.ch/groups/groupstraumann/papers/main.ps.gz

Contents

The triple GEM detector is a micropattern gas detector which consists of a primary ionisation
gap and three consecutive gas electron multiplier (GEM) foils [1]. A printed circuit board with
readout strips detects the current induced by the drifting electron cloud originating from the

last GEM stage. Thus the gas amplification and the signal readout are completely separated. Triple GEM detectors are being developed as a possible technology for the inner tracking in the LHCb experiment.

In an earlier note we have reported first experience with such a detector in a test beam at PSI[1] [2]. Here we describe the construction of an improved version (thinner transfer gaps, segmented GEM foils, two dimensional readout). Results from performance measurements are presented using intense hadronic beams as well as cosmic ray data.

1   Requirements on an inner tracking detector for LHCb

LHCb [3] is a second generation experiment on b quark physics which will be operated at the LHC (Large Hadron Collider) at CERN. The goal of the experiment is to measure systematically all observable CP violation effects and the rare decays in the B-meson system with unprecedented precision. It will allow to improve the knowledge on standard model physics and look for new CP violation effects possibly induced from physics beyond the standard model.

The analysis of rare B decay channels requires an excellent resolution of the kinematic quantities of the decay products, their momentum, invariant masses and vertex position. A beam axial magnetic spectrometer with a large, high resolution tracking system complemented with particle identification devices (RICH, electromagnetic and hadronic calorimeters and a muon system) provides optimal performance for B physics studies at LHC.

The tracking system consists of three parts: A vertex detector (silicon microstrip technology within the vacuum chamber of LHC), an outer tracking system to be installed in areas with small particle occupancies and an inner tracking system for areas with large particle occupancies. For the latter the collaboration recently decided among the various micropattern gas detector technologies to choose the triple GEM detector as described in this note. However this gas detector is still in competition with a microstrip silicon detector, the decision for one or the other of the two is presently foreseen to be made by end of the year 2001.

There are 11 inner tracking stations mounted vertically around the beam axis, each with a size of 60 cm (horizontal) × 40 cm (vertical). Momentum and invariant mass resolution ask for a position resolution of $\sigma < 200\mu$m, while the radiation length should be kept as small as possible (in the simulations so far a value of about 2% per station is assumed). A stereo angle of 100 mrad is foreseen and each station needs to provide 4 measurements: x, u, v, x, where u and v denote the stereo layers. For an efficient pattern recognition the channel occupancy has to be kept below a few %, which also requires the time occupancy of the signals not to exceed about two or three LHC bunch crossings of 25 ns.

Simulation of the LHCb interaction region, including the beam vacuum chamber, were performed to estimate the particle fluxes [4], using an average nominal luminosity of 2×10^{32} cm^{-2}s^{-1}. The peak luminosity is assumed to be higher by a factor 2.5. The particle fluxes and its compositions depend strongly on the position parallel to the beam axis z and on the distance from the beam: the maximum charged hadron rate is expected to be 8×10^3 mm^{-2}s^{-1} and the maximum electron and positron rate (originating mostly from photon interaction with the beam

---

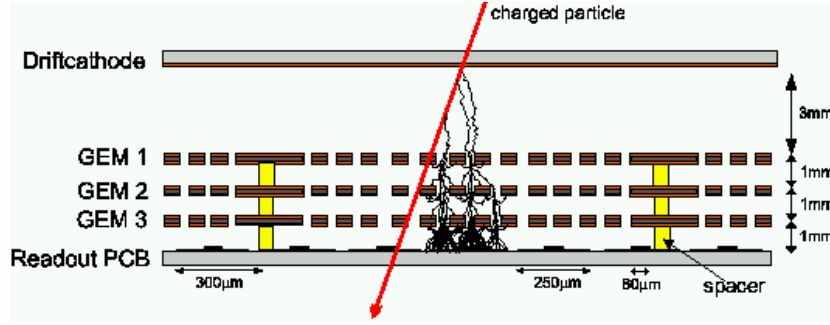[1]Paul Scherrer Institut, Switzerland. http://www.psi.ch

Figure 1: Schematic view of the detector with three GEM foils, which are seperated by 1 mm gaps using spacers. Pitch and width of the strips on the two coordinate readout board are also shown.

Figure 2: GEM foil with a 200 μm wide gap between segments, where the copper is removed.

Figure 3: A single spacer glued onto the GEM foil onto a hole free area.

pipe) might be as high as 5×10^4 mm^{-2}s^{-1}. A large fraction of the latter enters the detector under a large inclination angle. The total counting rate per station reaches between 200 and 1000 MHz, again depending on z. These rates correspond to a maximum total radiation dose of about 1.6 Mrad/year.

A major problem of gas micropattern detectors comprises the fact, that in hadronic particle beams from time to time very high primary ionisations occur, which may lead to high voltage breakdowns producing dead time, huge electronic noise to other detectors and even may damage the detector and the readout electronics. For GEM foils it has been shown, that they usually withstand several hundred sparks per cm^2 without permanent damage [5]. We require both, that the spark rate is limited to one per hour per tracking plane and the detector should stay alive for several years. Taking into account the expected hadron particle flux it follows, that the discharge probability per incident particle must not exceed 10^{-12}.

2   Detector construction

The triple GEM detector is depicted schematically in figure 1. The size of the active surface is 30×23 cm^2.

2.1   Drift gap and amplification stages

The drift cathode consists of a 50 μm thick Kapton foil covered with a 15 μm thick copper layer. The drift gap is 3 mm wide.

The gas amplification takes place in three stages in the holes of the GEM foils[2], which are mounted with a gap of 1 mm between them. The basis material for the foils is 50 μm thick

---

[2]The GEM foils were manufactured by Rui de Oliveira et al. in the CERN workshop

Figure 4: A GEM foil stretched with tape to a large auxiliary aluminum frame during glueing.

Figure 5: HV resistor connected to GEM segment, 1mm G10 frame and spacer.

Kapton with a 15 μm thick copper cladding on both sides. The hole parameters are chosen in accordance with results of studies made by the CERN GDD group [6]. The holes are arranged with a pitch of 140 μm, the diameter of the copper hole is 80 μm and the diameter of the hole in the Kapton is 50 μm (see also figure 2).

The capacity between the two electrodes of a GEM foil is as large as 30 nF. To reduce the total charge released in a high voltage breakdown the GEM electrode is divided on one side into 10 rectangular segments, which are separated by copper free gaps of 200 μm width. Within these gaps there are no GEM holes (figure 2). Each segment is powered through an individual HV resistor of 10 MΩ and 1 MΩ resistor for the first two and the last GEM foil respectively outside the detector. This segmentation has the additional advantage, that only a small fraction of the detector would fail in the unlikely case of a high voltage breakdown causing a permanent GEM short.

To avoid contact between two GEM foils due to electrostatic forces or other mechanical instabilities spacers are glued onto them about every 4.5 cm. Since HV breakdown problems may occur due to unintentionally deposited glue in the GEM holes, the GEM contains 2 mm diameter regions without holes, where spacers can be placed (see figure 3). The spacers consist of small cylinders with diameter 1.1 mm and height 1 mm of pure epoxy resin H72[3]. They are glued with the same epoxy resin onto the GEM foil. Each GEM is equipped with 35 spacers, which were positioned by hand under a microscope. This procedure took about 45 minutes per foil. The total fraction of inactive surface of the detector due to spacers is 1.6×10^{-3}, however the inefficency introduced is expected to be even smaller, since typical charge cluster diameters resulting from particle tracks are of order 0.5 mm.

The detector was mounted together starting with the drift cathode. An aluminum frame was glued mit the same H72 glue on the Kapton side and a 3 mm G10 frame onto the copper side simultanously. The aluminum frame is required to assure mechanical stability of the detector. In future this frame should be replaced by a full size plate of thin material (e.g. Rohacell) to reduce the total radiation length.

Then the GEM foil was stretched by putting it onto a large aluminum frame and pulling it with tape to the sides (figure 4) with the spacers already in place. Now a high voltage test in a nitrogen atmosphere was performed. The voltage applied to the foils was increased continously during about two hours until sparking started somewhere between 580V and 650V. The GEMs were kept sparking about twenty times before decreasing the voltage again to make sure that dust possibly trapped in the GEM holes would burn out without generating a short circuit between the GEM surfaces.

After this test was successfully completed the first GEM foil was simultanously glued to the 3 mm G10 frame and the first 1 mm frame onto the other side of this GEM. Afterwards the next two GEMs were stretched, tested and glued in the same way. An overview of a part of

---

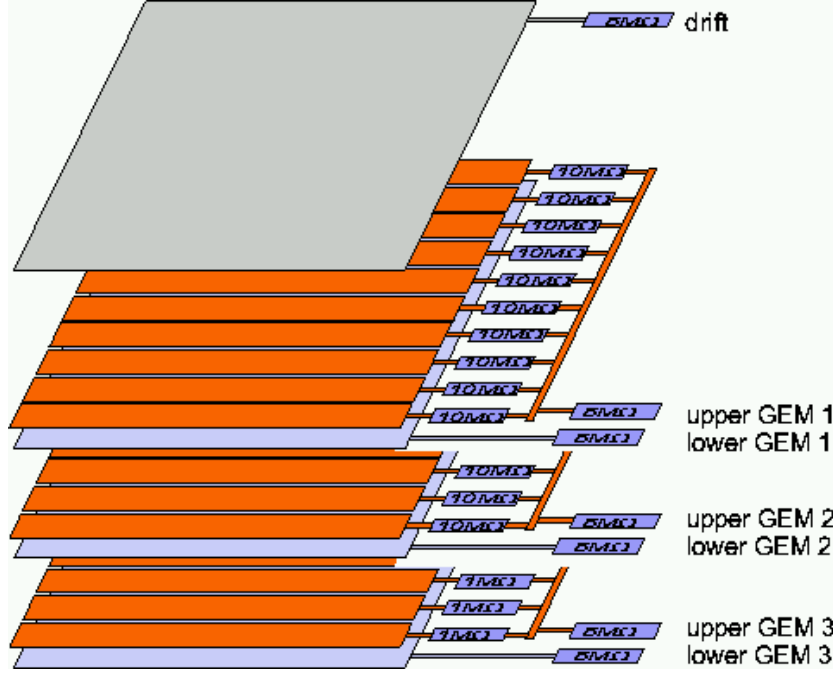[3]EPO–TEK H72, Polytek GmbH, D-76337 Waldbronn, Germany

Figure 6: HV-schema, each of the seven needed voltages is delivered by individually controllable power supply channels.

the detector in this state is shown in figure 5. Finally the hole sandwich structure was glued to the readout board.

2.2   High voltage supply

To allow for maximal flexibility in choosing the electrical fields that are needed to run the detector all high voltages are delivered separatly by an individually controllable power supply channel. The high voltage schema is shown in figure 6. The currents are monitored for each high voltage channel. A discharge in a GEM can be indentified by observing the reloading current of this GEM segment.

Of the two detectors built, one has the segmented GEM on the upper side as in figure 6, in the other detector the segmentation is on the side towards the readout board. No significant difference (e.g. in sparking probability) has been observed.

2.3   Two dimensional readout board

The separation of the amplifying stage from the readout stage in a triple GEM detector allows to use any readout pattern that is appropriate for the application. Here a two dimensional readout printed circuit board was chosen with a stereo angle of 5° between two sets of parallel strips. The rotated strips on the top are separated through a 50 μm Kapton layer from the lower strips (see figure 7 and figure 8). The lower strips have to be wider than the upper ones in order to collect in average an equal amount of charge on both layers (charge sharing). We
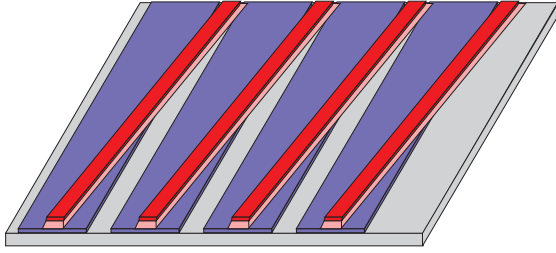
Figure 7: Schematic drawing of the readout board. Pitch 300 μm, upper strip width 60 μm, lower strip width 250 μm.

Figure 8: An optical microscope picture of the readout board.

have used 60 μm and 250 μm wide strips with a pitch of 300 μm for each plane. Although this pitch was chosen for practical reasons to connect the printed circuit board to a HELIX front-end chip, it turns out to be reasonable choice for such a detector (see the discussion of the results below). The length of the strips is 30 cm.

This readout board was manufactured from copper cladded Kapton foil with the same etching technology as the GEM foils in the CERN workshop. It is glued to a 100 μm thick G10 sheet to insure a reasonable flatness. Below the readout board a 4 mm thick Rohacell plate is mounted covered with a grounded aluminum foil, which acts as an electrical shield.

2.4   Readout electronics

The readout strips are connected to the HELIX 128 readout chip [7], originally developped for the HERA-B experiment. Each layer of a detector is equipped with 4 chips (= 512 read out channels). Two thirds of the active area of the detector can be read out this way.

The connection (see figure 9) is made through a short (3 cm length) Kapton stripline bonded with Z-bond glue[4] and a fan-in, which fits the pitch of the HELIX input pads of 41.4 μm. This fan-in is made of thin film ceramics[5] and includes a serial overcurrent protection resistor of 600 Ω to avoid damage of the preamplifier input in case of chamber sparks or shorts (optimised for the HERA-B MSGC operation).

The signal path is closed through the capacity between the lowest GEM and the readout board of about 500 pF.

The capacity of the ceramic fanin was measured to be 2 pF. The total capacity of the fully mounted system of one strip to all its neighbour strips and the full electrical environment measured by coupling a square wave pulse to the readout board (still connected to the HELIX) through a 1 kΩ serial resistor. From the observed rise time of this pulse a capacity of 86 pF was determined.

---

[4]done by Dr. U. Werthenbach University of Siegen
[5]manufactured by Siegert TFT, Hermsdorf, Thüringen

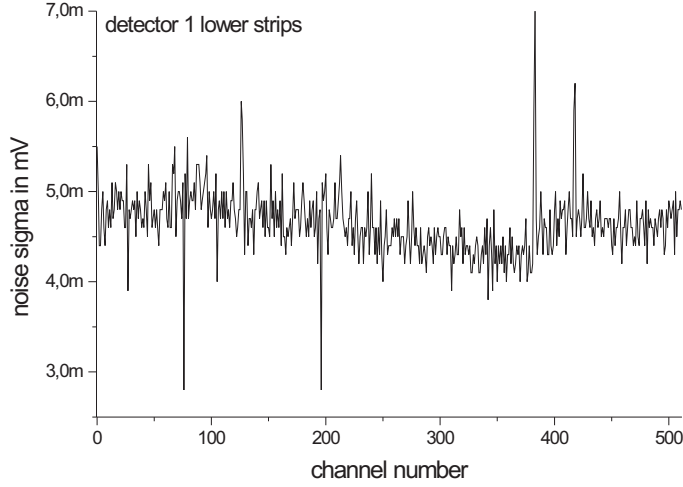Figure 9: HELIX boards connected to readout PCB via a Kapton fanout.

Figure 10: Noise distribution for the readout channels in one readout layer. Channels with lower noise indicate broken readout strips, bad connection to the electronics or damaged readout channels. A higher noise can indicate a short between readout strips.

By coupling a well defined charge to a readout strip the HELIX gain was measured to be 880 e$^-$/mV in this configuration. The average noise level (Figure 10) of 4.8 mV corresponds therefore to 4200 electrons. From this information and the HELIX data sheet a total capacity of the readout board of ≈ 100 pF was derived, which is consistent with the value above. In addition an electrical simulation of the setup gave similar figures on the capacity [8].

The HELIX comes in its analog characteristics very close to the chip, that will be used later in LHCb. The shape of the preamplifier output of the HELIX depends on the capacity of the detector connected to the input. For our detector it has a FWHM of about 90 ns. The amplitudes of these signals are sampled by a 10 MHz clock and are stored in the analog pipeline, that is included in the HELIX chip. The HELIX was run in standard conditions [7].

The 10 MHz clock was in general operated independantly of the particles traversing the chambers. Therefore the sampling time was not optimally set to the pulse maximum, but randomly distributed over 100 ns. The data used to measure the pulse height distributions were however taken with an additional trigger condition requiring the signal to be within 25 ns of the active clock edge.

After a trigger occurs each HELIX chip sends the analog value from all 128 channels multiplexed through one readout line, which were digitised by an oscilloscope connected to a PC via GPIB bus and controlled by LabVIEW. The communication between the oscilloscope and the PC limited the readout speed to 0.5 Hz. For cosmics data taking the scope was replaced by VME ADC boards.

The pedestal for each readout channel is subtracted offline and each signal is corrected for baseline variations (common mode noise) by using a filter to remove large period components from the data. In figure 11 the corrected data from a minimum ionising particle crossing the detector is shown. For identifying the signals a threshold of 3.5 sigma of the noise distribution
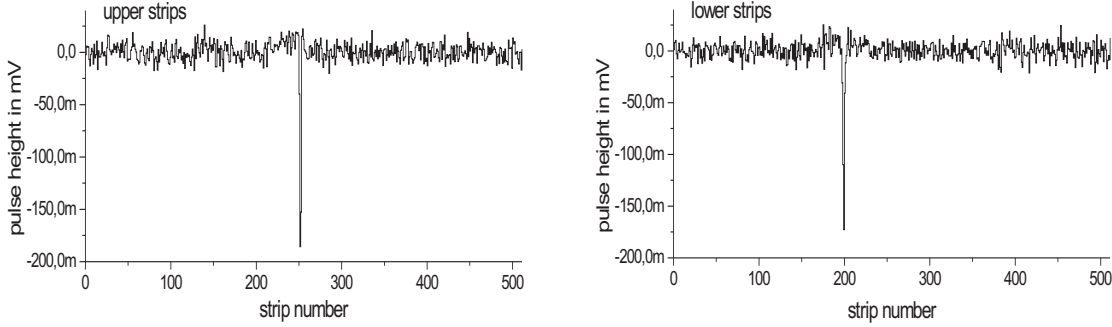
Figure 11: Corrected Helix data from a minimum ionising particle. The signals of the two readout coordinates as a function of the channel position are shown.
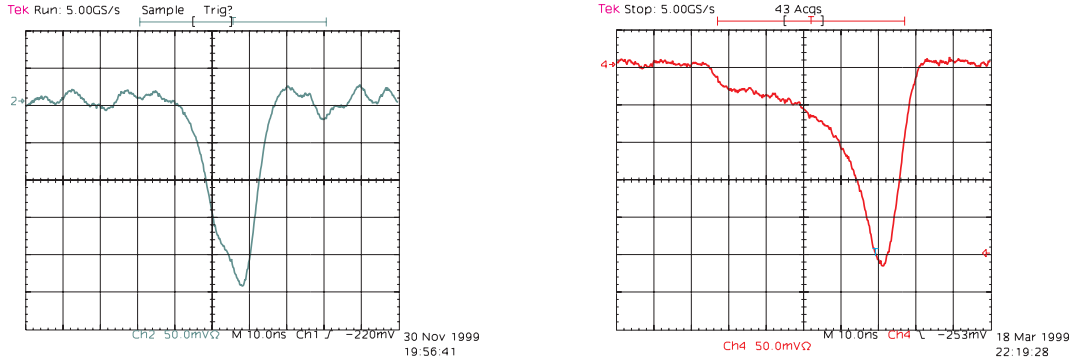

Figure 12: Left: signal shape for the new detector with 1mm transfer gap (8 strips connected together). Right: signal shape of the old detector with 3 mm transfer gap (5 strips connected together)

is applied.

2.5 Signal shape

In order to study the shape of the chamber signal a fast amplifier VV61[6] with a rise time of 0.5 ns was connected to the detector.

The signal from a Fe^{55} source is shown in figure 12 on the left. For comparison the signal of our previous prototype detector [2] with a transfer gap of 3 mm is shown on the right in the same figure. The pulse shape can be understood by interpreting the signal as the induced current due to the moving charged cluster in the gap between the lowest GEM foil and the readout board: the drift velocity in Ar:CO$_2$ (70:30) at 5 kV/cm is $\approx$7.5 cm/μs, corresponding to a drift time for the 3 mm gap of 40 ns. Although the total current should be constant, we can observe a rising signal due to the effect that the strips close to the center of the cloud see

---

[6]R. Rusnyak Physikalisches Institut der Universität Heidelberg

an increasing fraction of the total current, as the charged cloud moves closer to the readout board surface. This rise time is close to the expected 40 ns.

For the new detector the rising of the signal is barely visible, since the drift time in the 1 mm gap is expected to be about 13 ns only.

3 Operation and performance measurements

Two identical complete detectors were built and mounted back to back, such that the stereo angles are +5° and -5° compared to the vertical strips. The distance between the centers of the primary ionisation gaps is 17.9 mm (see figure 13 right) allowing a crude crossing angle determination of the observed tracks.

The detectors were operated both at PSI beams and in a cosmic ray setup.

3.1 High rate particle beam experiment

At PSI four other groups of the LHCb Inner Tracker collaboration tested their detectors simultanously in December 1999. Picture 13 (left) shows the triple GEM detectors mounted between the prototypes of the other groups.
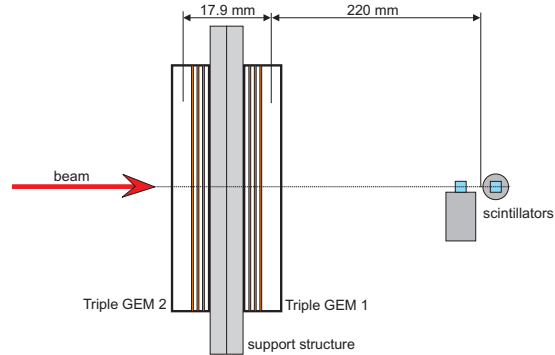

Figure 13: Left: setup at PSI in the πM1 area. Right: schematic drawing of the chamber arrangement and the scintillators.

Beam intensities and distributions were measured by a pair of 5×5 mm^2 scintillators mounted on a remotely movable table. The width of the beam was typically ≈6 cm. For operation stability tests a 350 MeV/c π^+ beam was used. The maximum achievable total rate was 60 MHz with a peak rate of 1×10^4 Hz/mm^2. For most of the data taking a 215 MeV/c π^- beam with low intensity (60 Hz/mm^2) was used.

3.2 Cosmic ray experiment

For a high statistics study of the performance as a function of the track crossing angle a cosmic ray setup was used. The chamber were mounted horizontally. A pair of 10×10 cm^2 scintillators were mounted below and above the detectors. To be able to study large clusters in detail the chambers were operated at a higher gain ($V_{GEM} = 390$ V) than usually.

3.3 Electrical field configuration

As an optimal HV setting the following values were exposed: drift field 3.0 kV/cm; transfer fields (between the GEM foils) 2.2 kV/cm; collection field 5.0 kV/cm. The most critical fields with respect to sparking are the two transfer fields. An increasing of these fields from 2.2 kV/cm to 3.0 kV/cm lead to an enhancement of the sparking probability by a factor of 10.

At the beginning the detector was operated with a drift field of 2.0 kV/cm. Later we discovered that an increase to 3.0 kV/cm causes a gain reduction of 15 %. This is qualitatively explained by a better transparency for lower drift fields: in the optimal case all field lines from the drift cathode are focused and compressed through the holes terminating on the readout board. According to simulations in the symmetric case a typical transparency for the primary electrons of 88% [9] can be reached in our configuration. By increasing the drift field some field lines terminate on the GEM foil and primary electrons are therefore lost.

It was observed, that the sparking probability is also reduced by about a factor of three with higher drift field corresponding to the lower gain of the chamber (see section on gain and spark probability). In contrast to that, the collection field between the lower side of the last GEM foil does not seem to influence the sparking rate.

After the amplification process in a GEM hole a major part of the electrons is lost to the lower GEM side. If the field on the lower side is increased, more electrons can be collected to the readout board (*collection efficiency*). On the other hand a high collection field may cause sparks to propagate to the readout board and may damage it. Because of the robustness of the readout board and the well proven high voltage protection of the HELIX readout electronics, we decided to increase the collection field to 5.0 kV/cm.

According to simulations the collection efficiency in this configuration for the upper and middle GEM is 42 %, for the lowest GEM 62 %. Taking into account in addition the primary electron transparency and the loss due to attachment in the gas, the total fraction of all primary and secondary electrons collected on the readout board is only 7.5 % [9].

3.4 Detector signal gain and spark probability

The detector is operated with Argon and CO_2 gases with a mixing ratio of 70:30. Although CO_2 alone is not a very stable quencher gas, the simpler infrastructure with respect to safety and the chemical ageing stability of this mixture outweighs a possible improvement in discharge performance of more complex quencher gases. The primary ionisation gap has a width of 3 mm, where in the Ar:CO_2 70:30 gas mixture a vertically incidenting minimum ionising particle produces in average 21 primary electrons in about 8 clusters [9].

The detector gain (see figure 14) was measured in various different ways.

The total incident particle rate was calculated by measuring the coincidence rate of the two scintillators moving them along x and y across the beam cross section. The anode current was determined by measuring the current in the ground lines of the preamplifiers and it was verified, that this is the same value as the sum of all upper and lower GEM currents and the drift current taking the proper sign into account. From this current and the assumption of 21 primary electrons per minimum ionising particle the detector gain was calculated.
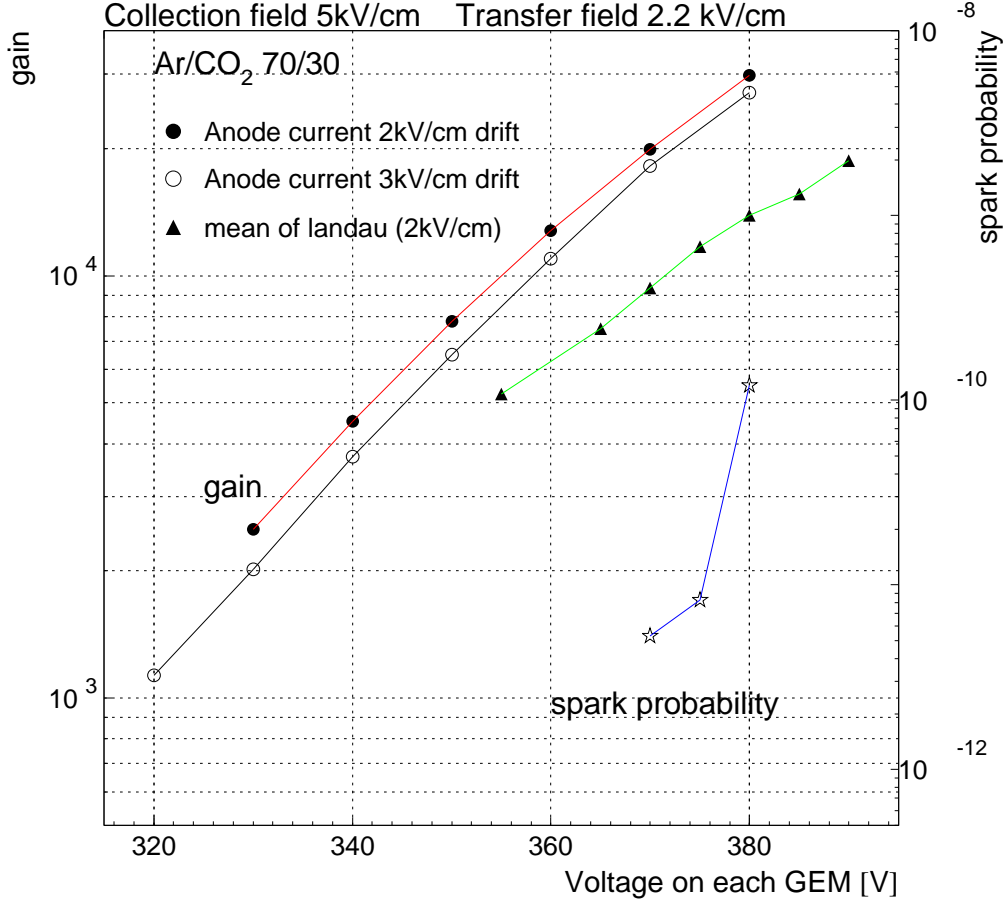
Figure 14: Detector gain, determined with different methods, as a function of GEM voltages, where all three GEM are set to the same voltage. Also shown is the spark probability per incoming particle

Due to a possible missalignment of the scintillators against each other an overestimation of the rate of 20 % is possible. The exact shape of the beam varies with details in the beam line settings giving rise to a further systematic uncertainty of about 20 %.

The gain was also determined from a Landau distribution fitted to the pulse height spectra (see section on results) and the known gain of the electronics chain taking into account the charge sharing between the two readout coordinates.

Furthermore signals of an Fe^{55} γ–ray source were observed in the chamber resulting in gain values between the two previously mentioned. In summary, considering the various uncertainties we believe, that the correct signal gain is located somewhere between the two curves in figure 14.

When turning on the detector the gain observed is initially lower and slowly increases with time during irradiation with a source. After a few minutes the signal size becomes stable at

about double of the initial value. This is interpreted as charge up of the Kapton surface in the GEM holes and has been seen by many other groups as well [10].

The spark probability per particle was measured at 350 MeV/c beam energy (see figure 14). The maximal beam intensity was 60 MHz. For example 45 sparks were observed in both detectors in 12.5 hours at a GEM voltage of 375 V, resulting in a spark probability of 8.3×10^{-12}.

4 Results

4.1 Analysis procedures

After the detector signals were digitised and stored on disk the analysis proceeds in an offline procedure with the following steps:

1. Baseline correction and subtraction as described in the section of readout electronics.

2. Applying a threshold of 3.5 times the average noise. Each channel is treated seperately. Signals exceeding this threshold are identified as a cluster.

3. The center of gravity and both the root mean square of the width and the number of channels above threshold of these clusters are determined. For the PSI data in addition a Gaussian fit to each signal gives the width of the cluster in terms of σ in units of strips.

4. In cases, where there is exactly one cluster in each plane, the x and y coordinates are calculated from the center of gravities. This works only for the low rate data at PSI and for cosmics.

4.2 PSI data

4.2.1 Pulse height and efficiency

Figure 15 shows the correlation between the pulse heights of the two readout coordinates as determined from low rate PSI data. In average the signals on the upper strips are $\approx$1.25 times larger than those of the lower ones.

Figure 16 demonstrates, that the pulse height distribution can be well fitted by a Landau type function reflecting the pulse height variations due to primary ionisation statistics. These distributions were used to determine the gain (see section on chamber gain).

Counting the number of non empty events for each scintillator trigger and variing the GEM voltages allows to determine an efficiency plateau for each of the four available planes (two chambers with two readout coordinates each), one of those is displayed in Figure 17.
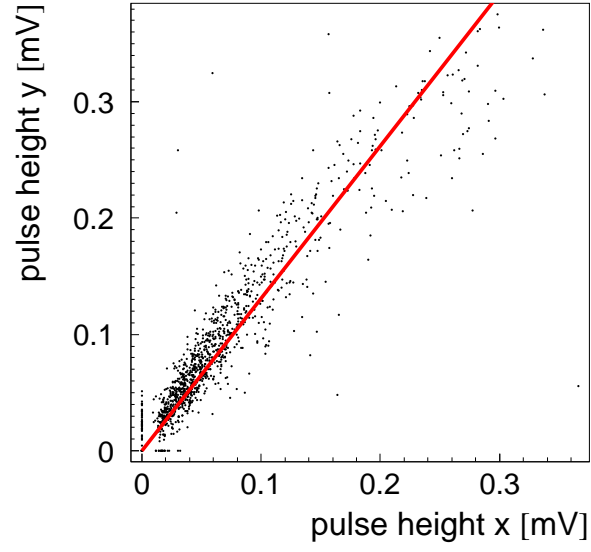
Figure 15: Correlation between pulse heights of the lower (x) and upper (y) strips.
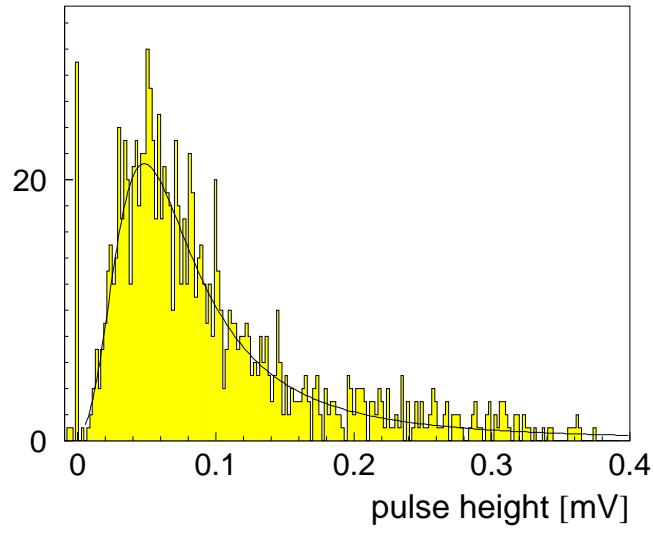

Figure 16: Pulse height distribution measured at a GEM voltage of 380 V. Signals below the threshold are filled into the bin at zero.
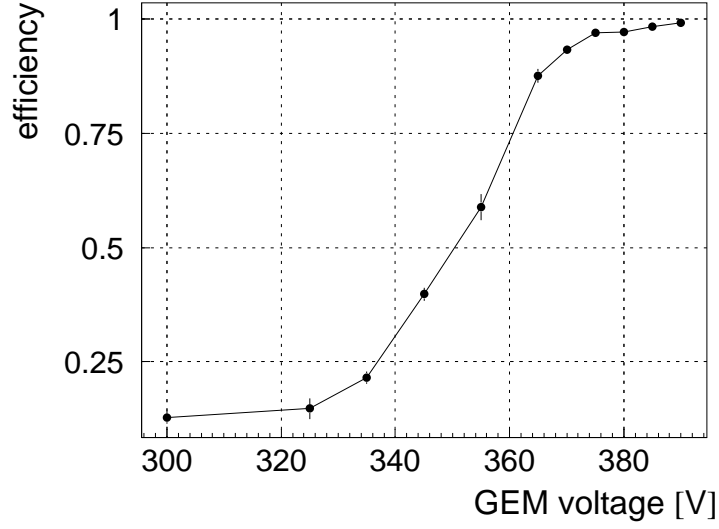
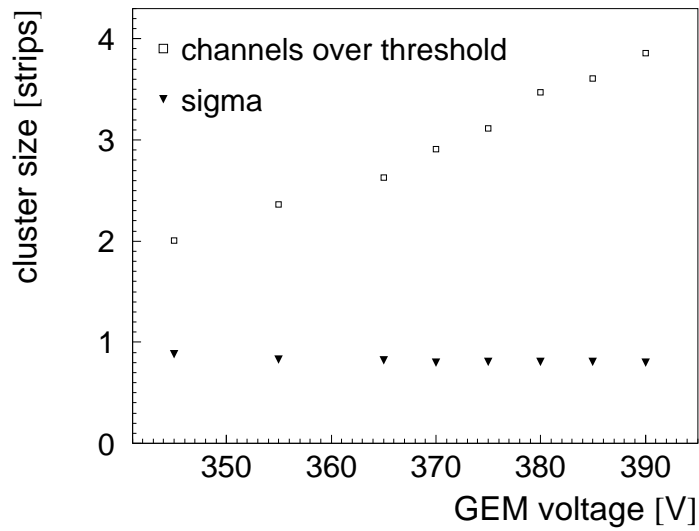Figure 17: Efficiency as a function of the GEM voltage.

Figure 18: Cluster width as a function of detector gain, determined from the number of channels above the 3.5 sigma noise threshold (open squares) and from the width of a Gaussian fit to the pulse shape (triangles).
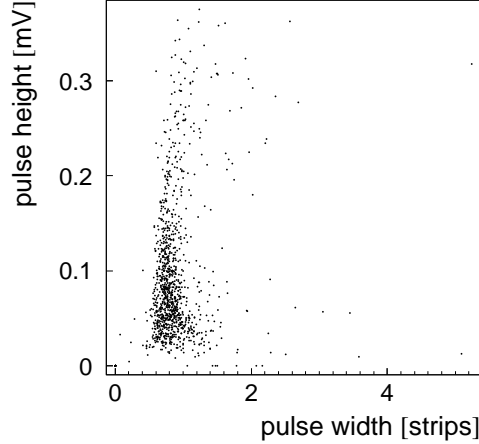
Figure 19: Correlation between pulse width and height. To determine the width of the signal a Gaussian fit was used.

4.2.2 Cluster size

The width of the signal was studied as a function of the GEM gain. In figure 18 two different methods of determining the cluster size are compared. An often used definition just uses the number of channels in the cluster, which have a signal larger than the noise threshold. This quantity clearly depends on the pulse height and as expected the average values rise with the gas gain.

A more physical definition of the cluster size uses the σ of a Gaussian fit to each pulse. Figure 18 shows, that this cluster size does in fact not depend on the gain of the chamber. The value of 0.8 strip pitches (240 μm) is consistent with an estimation, which is based only on the transvere diffusion ($D_t \approx 300 \ \mu\text{m}/\sqrt{\text{cm}}$) of the charged cloud along an average drift length of 4.5 mm.

In addition the cluster size (using the σ from the Gaussian fit) is correlated with the pulse height. A substantial electronic crosstalk between neighbouring readout strips would manifest itself in an increasing width for larger pulses. Figure 19 indicates, that there seems to be no problem with electronic crosstalk.

4.2.3 Resolution

Although 215 MeV/c π's give large multiple scattering and are therefore not suitable to do a resolution measurement, the differences between the coordinates measured by the two detectors are plotted as a cross check in figure 20. It shows that the alignment of the two detectors is well understood in both coordinates. A Gaussian fit gives $\sigma_x \approx 0.25$ mm and $\sigma_y \approx 1.3$ mm. Multiple scattering in the first chamber contributes about 0.1 mm to these values, while the angular divergence of the beam is estimated to be below 20 mrad, an upper
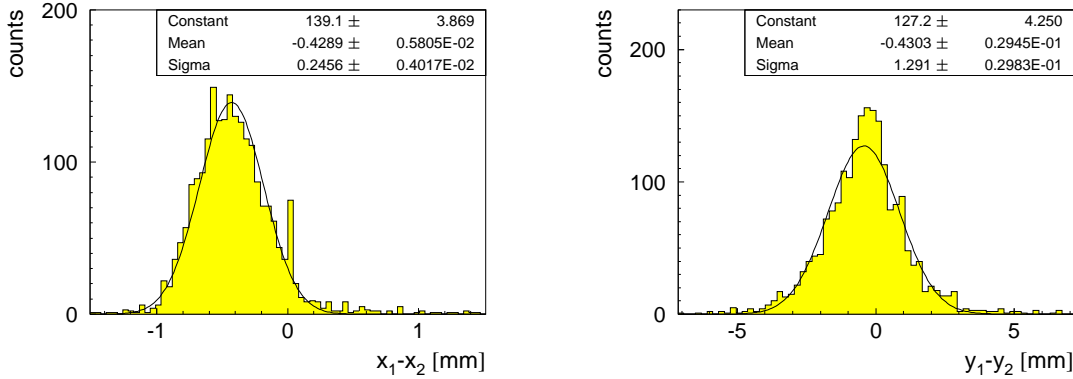
Figure 20: Difference between the x-coordinate (left) and the y-coordinate (right) of the two detectors, measured at 370 V GEM voltage

limit of its contribution is therefore 0.36 mm indicating, that σ_x is dominated by this beam divergence. For a real spatial resolution measurement a better defined beam of higher energy is obviously needed.

4.3 Cosmic ray data

With the identical detectors also cosmic data was taken. In figure 21 the channel map for the lower and upper strips is shown. Figure 22 shows the reconstructed hits of all recorded cosmic data. To cover a larger area of the detector the scintillators were moved gradually in y-direction. The distinct region with no hits corresponds to a disconnected GEM segment. Broken and hot channels (masked off) are clearly recognised.

4.3.1 Signal homogenity

The homogenous irradiation of the chamber with high statistics allows to observe variations in the signal size in different regions of the chamber. In general the detectors behave rather homogenous, however closer to the borders of the active region the signal size starts to drop down to about a half of its value compared to the center of the detector (see figure 23). Similar reductions in signal size have been observed on all chamber boundaries.

There is a suspicion, that the copper and the Kapton GEM holes might be badly aligned to each other at the border of large surfaces due to stability problems of the film masks [11].

4.3.2 Track inclination

In the LHCb application the distribution of the inclination angle of the dominating background particles (mainly electrons and positrons) is very broad. It is therefore interesting, how the signals depend on the polar angle of the incident particle.
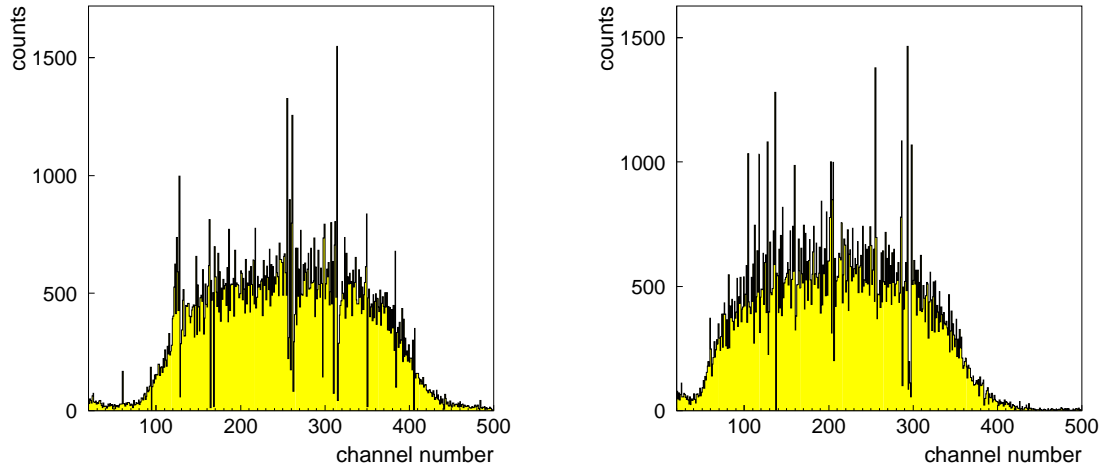
Figure 21: Channel map of lower (left) and upper strips (right).

Figure 22: Hit map of recorded cosmic data. Broken strips are clearly visible.
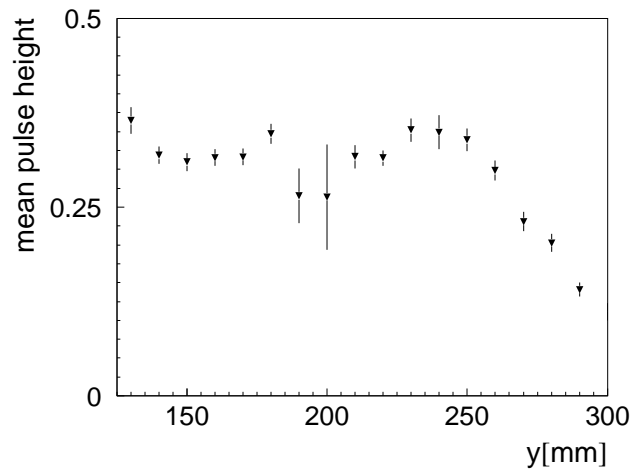

Figure 23: Signal gain homogenity. The average pulse height is shown as a function of the position. At $y = 300$ mm the frame of the chamber is located.
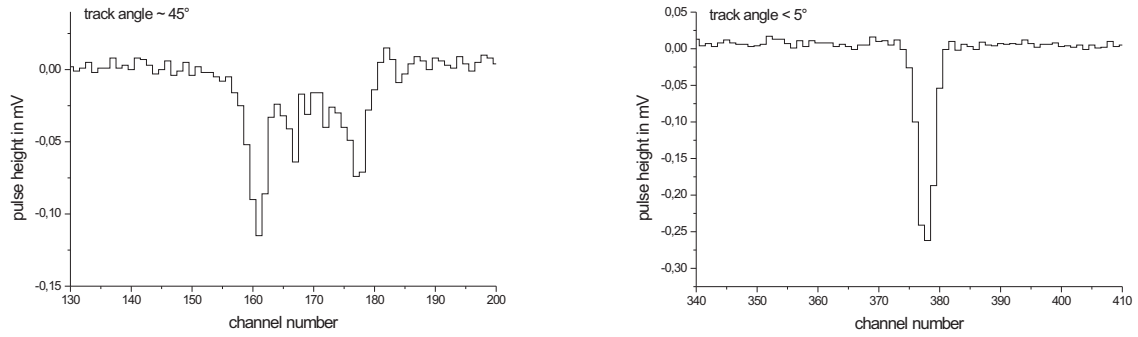
Figure 24: The signal size as a function of strip position for a single cosmic ray event with an inclination angle of about 45° (left). For comparison the figure on the right shows a signal from a vertically incidenting track.
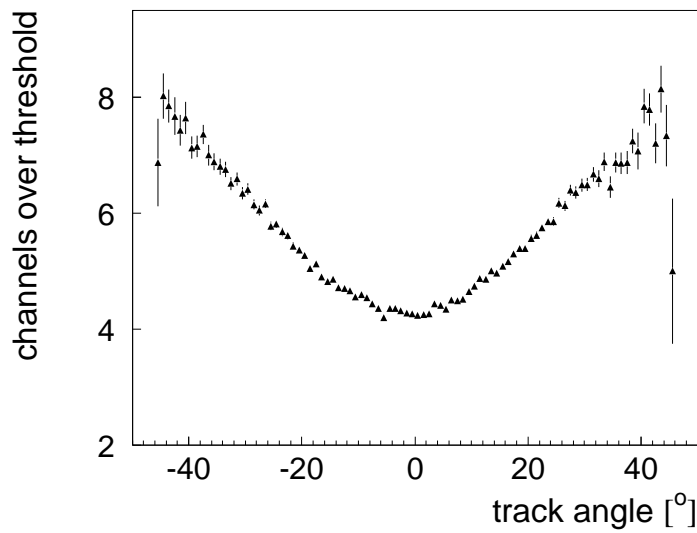

Figure 25: The clustersize of the cosmic ray data as a function of the inclination angle.
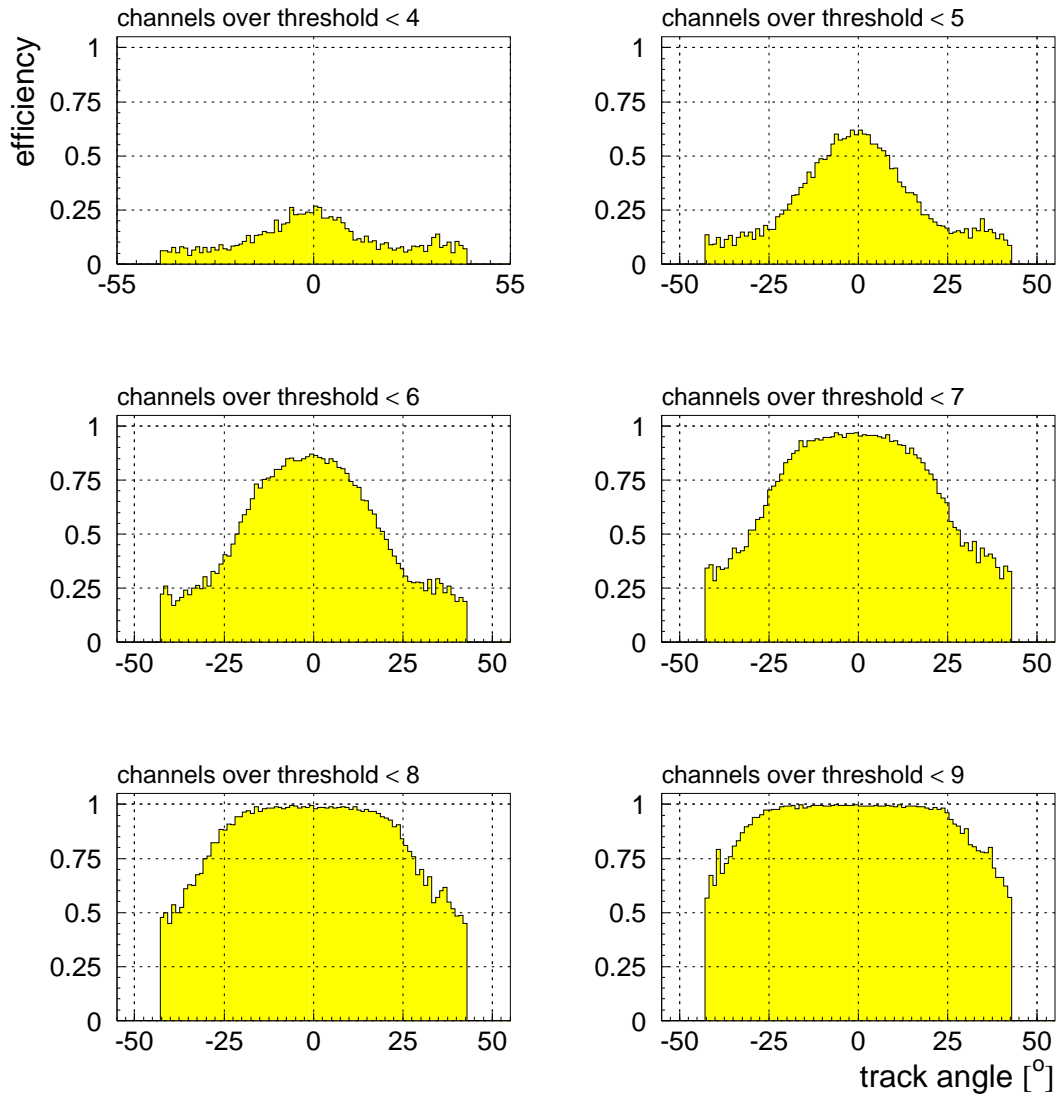
Figure 26: Detector efficiency as a function of track inclination angle for different threshold cuts in ADC units

The cosmic ray sample is well suitable to study this question: from the position information of the two detectors the inclination angle of the incoming cosmic particle was reconstructed, and the events were studied as a function of this angle.

Figure 24 shows the signal of a cosmic ray event observed under an angle of about 45° compared with a normal, vertical incidenting track. The cluster is wider as expected since the tracks crosses several drift cells. The signal height varies according to the primary ionisation statistics. Due to the smaller number of clusters for each cell this variation is much bigger than for a normal signal. This leads to the difficulty that from the signal alone it is impossible to decide whether the event originates from a single, inclined track or from several vertical particles. In a high rate application additional tracking information from other devices would be needed to analyse the data.

Figure 25 shows the correlation of the total width of the signals with the inclination angle of the track, which behaves as expected.

In principle it would be thinkable, that this feature could be used to suppress the low angle background already on the chamber level by cutting on the cluster width. In figure 26 the efficiency for tracks as a function of the inclination angle for different such cuts shows, that this method in principle works. By choosing a threshold of 7 the efficiency for tracks with an angle larger than 30° is reduced by a factor of three without loosing too much efficiency at the nominal inclination angle of 0°.

However this feature depends so critical on the cut value, that even small instabilities in the signal size of the chamber would have big effects on the background acceptance or even on the efficiency of the nominal tracks.

5   Conclusions

Large triple GEM detectors have shown stable operation in the worst hadronic beam environment at PSI, giving a large signal gain of more than 10^4 with spark probabilities per incoming π below 10^{-10}.

By using a "zig-zag" geometry of the readout board its capacity could be reduced by a factor three to four, which would proportionally reduce the thermal noise of the preamplifier, thus allowing to run the chamber with a gain of about 5000, where the spark probability is far below 10^{-12}.

This very high rate capability is supported in addition by an intrinsically very fast signal response without showing any "ion tail" in the detected signal.

The cluster size is comparable with expectation from the transverse diffusion of the charge cloud. The FWHM diameter of the signal at the readout board of about 0.5 mm allows in principle very accurate position measurements with typical readout line pitches of 0.3 mm, to be measured in a future test beam setup with high energy particles. But for very high rate application this large clustersize can result in significant channel occupancy.

Reducing acceptance of low angle tracks by cutting on the clustersize works in principle, but the efficiencies are very sensitive to the actual cut value.

In summary the triple GEM detector is a very stable, robust, low X_0, fast and cheap detector for applications with intermediate size areas and very high, even hadronic particle densities, showing lowest sparking rates at very high gains compared to other technologies. Low angle tracks should be avoided. Significant safety factors for the gas gain should be used to compensate for inhomogenous signal size across the chamber. If analog readout is used a very high accuracy in track position measurement can be expected.

References

[1] F. Sauli: *The Gas Electron Multiplier (GEM)*, Nucl. Instr. and Meth. A 386 (1997) 531-534

[2] M. Ziegler, P. Cwetanski, U. Straumann: *A triple GEM detector for LHCb*, LHCb public note 99-024, June 30, 1999.

[3] LHCb technical proposal, CERN LHCC 98-4, 20 February 1998.

[4] V. Talanov: *Radiation environment at the LHCb innner tracking area*, LHCb public note 2000-013, May 28, 2000.

[5] J.P. Perroud, results from a GEM spark test with α particles, private communication.

[6] S. Bachmann et al.: *Charge Amplification and transfer Processes in the Gas Electron Multiplier*, CERN-EP /99-49

[7] HELIX Manual
http://wwwasic.ihep.uni-heidelberg.de/~feuersta/projects/Helix/helix.ps.gz

[8] L. Shekhtman, Novosibirsk. Private communication in the LHCb inner tracking meeting, CERN, March 17, 2000.

[9] P. Cwetanski: *Studies on detector prototypes for the inner tracking system of LHCb*, Diploma thesis, Universität Heidelberg, March 2000.

[10] M. Hildebrandt: *Entwicklung und Bau der Detektoren fr das Innere Spurkammersystem bei HERA-B*, Ph.D. thesis, Universität Heidelberg, April 1999.

[11] L. Ropelewski, CERN, private communication.